RSC Advances

ROYAL SOCIETY OF CHEMISTRY

www.rsc.org/advances

Table of contents entry:

Hybrid micro/nanotopographic features are of crucial importance to the activity of osteoblasts.

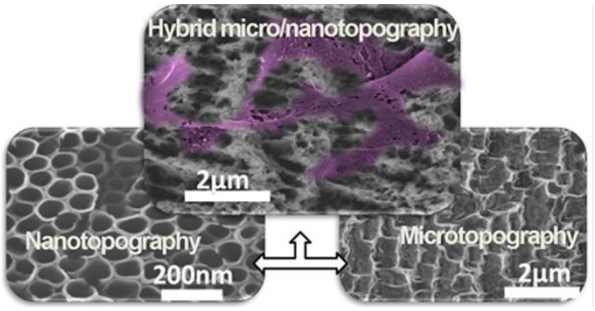

Journal Name

ARTICLE

Synergistic effects of hierarchical hybrid micro/nanostructures on the biological properties of Ti-based orthopaedic implants

Received 00th January 20xx,
Accepted 00th January 20xx

DOI: 10.1039/x0xx00000x

www.rsc.org/

B. E. Li, [a]† Y. Li,[b]† Y. Min, [a] J. Z. Hao, [a] C. Y. Liang, [a] H. P. Li, [a*] G. C. Wang,[c,d*] S. M. Liu,[e] H. S. Wang [a]

A hierarchical hybrid micro/nanostructure was produced on the surface of titanium (Ti) implants by combined use of acid etching and anodic oxidation. The bioactivity of the modified Ti was evaluated by a simulated body fluid (SBF) soaking test and *in vitro* cell culture experiments. The results showed that the surface-modified Ti implants had a microstructure w enhanced surface roughness. There was also a nanostructure superimposed on the microstructure, forming a hierarchical hybrid micro/nanostructure. The modified Ti accelerated the Ca-P mineralization deposition on their surface in SBF, and promoted osteoblast adhesion, proliferation, and bone-related gene expression compared to the polished Ti and the Ti implants subjected only to acid etching or anodic oxidation, which was ascribed to the synergistic effects of both micro- and nanotopography generated. This study provides a simple and cost-effective approach to enhance the bioactivity and biocopatibility of orthopaedic implants, and points out the importance of both micro and nanotopography.

Introduction

Titanium (Ti) is the most commonly used dental and orthopedic implant material in clinics because of its excellent biocompatibility and mechanical properties. Although Ti-based devices have achieved high success in improving the life quality of aged or injured individuals, implant failures owing to poor osseointegration still frequently occur due to their bioinertness,[1] which limits the wide application of Ti-based implants.

The physical structure of biomedical implants is now known to be one of the key factors in determining their biological performance. Both micrometer [2,3] and nanometer [4–6] scale topographic features of the implant have been proved to significantly influence the *in vitro and in vivo* cell behaviors, such as cell morphology, migration, adhesion, proliferation and differentiation. Studies have shown that microtopographies increased bone-to-implant contact and enhanced the adhesion and proliferation of osteoblasts.[7,8] Implants with microtopographies have already been clinically used and good clinical performances have been evidenced.[9] Nanotopography can also enhance the biological performance of biomedical implants.[6,10] For instance, osteoblast proliferation was observed to be significantly enhanced on the nanostructured alumina, titania and hydroxyapatite ceramics in comparison to their conventional counterparts.[11]

Due to this well-proved beneficial effect of micro- and nanotopography on the biological performance of implants, surface topography modification at both micron and nanoscale level becomes one of the dominant approaches in the biomedical field to improve the osseointegration of orthopaedic and dental implants. [8,12-14] For example, Kubo and coworkers[13] produced micro- and nanostructures on a Ti surface by sputtering titania nanonodules on a microscale architecture created by acid etching. Xie et al.[14] fabricated micro/nanostructured implants through anodic oxidation and plasma spraying. The obtained micro/nanostructures have been proved to induce hydroxyapatite formation in simulated body fluids (SBF) and enhance the cellular attachment, spreading, proliferation, and differentiation. However, these coatings have the potential to form wear debris when used under load-bearing conditions, which can be harmful to the osteoblasts,[15] moreover, the fabrication process is time-consuming and costly. Thus, alternative methods to produce well-defined micro/nanostructures on Ti implant surface are highly desired.

Acid etching using HCl, H_2SO_4, HNO_3 and HF is an effective method for producing micropores on a metal surface. Microporous surfaces with a pore diameter of 0.5–2μm could be obtained on a Ti surface through acid etching. However, it should be noted that the corrosion resistance of the implant deteriorates due to the significant increase in the specific surface area, which may result in higher amount of metal ions released into the physiological fluids from the metal, and thus inducing resultant cytotoxicity.[7] Various methods of surface

[a] *School of Materials Science and Engineering, Hebei University of Technology, Tianjin 300130, China.*
[b] *Stomatological Hospital, Tianjin Medical University, Tianjin 300070, China.*
[c] *Soft Matter Nanotechnology Laboratory CIC biomaGUNE, Paseo Miramón 182, Donostia-San Sebastian 20009, Spain.*
[d] *Research Center for Human Tissues and Organs Degeneration, Shenzhen Institute of Advanced Technology, Chinese Academy of Science, Shenzhen 518055, China.*
[e] *Department of Gem and Material Technique, Tianjin University of Commerce, Tianjin 300134, China.*
† Baoe Li and Ying Li contributed to the work equally.
Electronic Supplementary Information (ESI) available: [details of any supplementary information available should be included here]. See DOI: 10.1039/x0xx00000x

modification have been being developed to produce oxide layers with a better chemical inertness on the metal surface to inhibit the ion release.[16] Among them, anodic oxidation is an economical, simple, and versatile technique to produce oxide layers on a variety of metals and alloys (e.g. alumina, Ti-based alloys).[11] The anodized surface has been proved to improve the corrosion resistance or wear resistance of the metal implants [5,6]. In recent years, this method has also been widely applied to produce uniform and controllable nanostructured titania on the implant surface.[6]

In this study, biomimetic hierarchical micro/nanostructured topographies were produced on the surface of Ti implants through the combination of acid etching (to produce a microstructure) and anodic oxidation (to form a nanotubular oxide layer). The biological properties of the modified Ti implants were evaluated by simulated body fluid (SBF) soaking test and *in vitro* cell culture experiments. Ti implants with microstructure only, nanostrucuture only and neither microstructure nor nanostructure were also prepared by acid etching, anodic oxidation and polishing, respectively, and used as control groups.

Experimental

Specimen preparation

Pure Ti (10mm×10mm×1mm) was used as the substrate. After polishing with #1000 SiC sandpapers and ultrasonic cleaning in acetone, ethanol and deionized water, the polished Ti substrates were immersed in 3 wt.% HF solution for 2 minutes to dissolve the air-formed oxide film on their surface (hereafter, referred to as polished Ti). Some of the polished Ti samples were further etched in a 66% H_2SO_4 solution for 5 minutes at 80℃ to form microscale topographic features (hereafter, referred to as Micro-Ti). With further anodization in the electrolyte of ethylene glycol containing 0.4 wt% NH_4F using a direct current (dc) voltage source (WYK-150, Yangzhou, China), Ti samples with a hierarchical hybrid micro/nanostructured surface were obtained (hereafter, referred to as Micro-nano-Ti). The anodization was carried out under a constant voltage of 20V at room temperature for 3 hours. A graphite electrode (40mm×40mm×5mm) was used as a cathode. The distance between the anodic and the cathodic electrodes was 40mm. After anodization, the samples were rinsed with deionized water and air-dried for further uses. For comparison, some of the polished Ti samples were subjected to anodization without acid etching to form a surface with only nanostructures (hereafter, referred to as Nano-Ti), and used as a control group.

Surface characterization

Surface morphology of the Ti samples was observed using scanning electron microscopy (SEM, HITACHI S-4800). And the surface chemistry was measured by energy dispersive spectroscopy (EDS) that attached to SEM. PHI-5800 X-ray photoelectron spectrometer (Physical Electronics, MN, America) was also used to characterize the changes in the surface chemistry after the surface treatment. XPS analyses were performed using a monochromatic Al Kα X-ray source (1486.6eV) with an Omni Focus III small area lens and multi-channel detector. Survey spectra were collected from 0 to 1100eV with a pass energy of 187.85eV, and high-resolution spectra were collected for Ti2p and O1s peaks with a pass energy of 10eV. All spectra were referenced by setting the C1s peak to 284.6eV to compensate for residual charging effects. The surface roughness was examined by atomic force microscopy (AFM, Agilent 5500), and the hydrophilicity was assessed through contact angle measurements using deionized water, which was conducted at room temperature. Briefly, a drop volume of 2μL was used to avoid gravitation-induced shape alteration. The drop image was acquired using a digital camera (1280×960 pixels) attached to the contact angle microscope and processed by an image analysis software.

Bioactivity evaluation

The samples were soaked in 30ml of SBF at 36.5℃ without stirring to evaluate their bioactivity. The ionic concentrations in SBF are nearly equal to those in human blood plasma. The SBF was prepared by dissolving analytical grade chemicals including NaCl, $NaHCO_3$, KCl, $K_2HPO_4.3H_2O$, $MgCl_2.6H_2O$, $CaCl_2$, and Na_2SO_4 into distilled water and the pH was adjusted to 7.4 at 36.5℃ with 45mM trimethanol aminomethane ($(CH_2OH)_3C(NH_2)$) and 1M HCl.[17] After soaking for 2 weeks, SEM and XRD were used for the surface morphology observation and phase composition analysis.

Biocompatibility evaluation

Cell morphology and proliferation

The samples were sterilized using an autoclave sterilizer at 121 ℃ for 30min before cell culture test. Murine preosteoblasts (MC3T3-E1, Tianjin Medical University, China) were used to evaluate the biocompatibility of the samples. They were cultured in the Dulbecco's modified Eagle's medium (DMEM, Gibco BRL, Grand Island, NY, USA) supplemented with 10% fetal bovine serum (Hyclone, Logan, UT, USA) and 3% penicillin/streptomycin. Culturing was carried out at 37℃ in an incubator in a fully humidified atmosphere of 5% CO_2. Cells were seeded on the sample surfaces at a density of 1×10^4 cells/cm^2. After culturing for 1, 4 and 7 days, the cellular proliferation on the sample surfaces was evaluated using MTT colorimetric assays (3-[4,5-dimethylthiazol-2-yl]-2,5-diphenyltetrazolium bromide, Sigma, St. Louis, MO) according to the manufacturer's instructions.[18] To observe the cellular attachment on the sample surfaces, the cells adhered on the sample surfaces were fixed for 4 hous with 2.5% glutaraldehyde in phosphate-buffered saline (PBS, pH =7.4), and then rinsed with PBS twice, followed by dehydration in a graded ethanol series and critical point drying. The samples were gold-sputtered prior to SEM observation.

Osteogenic gene expression analysis

After cells were cultured on the Ti surfaces for 7 days, total RNA was isolated from cells using a monophasic solution of phenol and guanidine isothiocyanate (Trizol, Invitrogen Life Technologies, Carlsbad, CA, USA), following the instructions of the manufacturer. RNA was quantified at 260nm using a Nanodrop spectrophotometer (NanoDrop Technologies, Wilmington, USA) and then reversely transcribed to cDNA using NI-RT Master Mix cDNA Synthesis kit (NEWBIO industry, Tianjin, China) that contains oligo (dT) in a final volume of 20μl to evaluate the gene expression.[5] Each cDNA was diluted 1:10 with RNase-free water, and then frozen (-20℃) until the PCR reactions were carried out.

Reverse transcription-polymerase chain reaction (RT-PCR) was carried out using the SYBR Green PCR reagent (Qiagen, USA) with the primer sets listed in Table 1. The length of the resulting amplicons and the GeneBank accession number were also shown in Table 1. Highly purified gene specific primers for bone sialoprotein (BSP) and the housekeeping gene, glyceraldehyde-3-phosphate dehydrogenase (GAPDH), were synthesized commercially (Shengong, Shanghai, China). Levels of each mRNA were normalized to that of GAPDH mRNA. The PCR products were electrophoresed on 1.5% agarose gels and stained with ethidium bromide to determine their sizes.

To determine the exact gene expression amount between different groups, real-time PCR was also performed using the SYBR green detection by Applied Biosystems 7500 Fast Real-Time PCR System (Applied Biosystems, Foster City, USA). For quantitative PCR, 10μL Real Master Mix SYBR green I (NEWBIO industry, Tianjin, China), 0.4μL forward and reverse primer, and 4.0μL cDNA template were used in a final reaction volume of 20μL. The thermal profile for all reactions was set as follows: 30s at 95℃, followed by 40 cycles of 5s at 95℃ and 30s at 60℃. Data collections were enabled at 60℃ in each cycle. The threshold cycle (Ct) was calculated by the instrument software. The mRNA value of BSP was normalized to that of the house keeping gene, GAPDH. Results are reported as relative gene expression ($2^{-\Delta\Delta Ct}$).

Statistical analysis

Samples were run in quintuplicate for each group. The data were presented in the form of mean ± standard deviations (SD). Statistically significant difference was determined by Students t-test. A *p*-value less than 0.05 was considered significant.

Results and discussion

Figure 1 shows the surface morphologies of the polished Ti, Micro-Ti, Nano-Ti, and Micro-nano-Ti. The polished Ti showed a relatively smooth surface (Fig. 1a). After acid etching, the surface of the Micro-Ti sample showed a microstructure composed of microsized pits, with a peak-to-peak distance of 0.5–5μm and a peak-to-valley distance of around 300nm (Fig. 1b). By contrast, a nanostructure consisting of well-organized nanotubes were found on the Ti surface only subjected to anodic oxidation. The inner diameter of the nanotubes was about 70nm, the wall thickness was around 5nm (Fig. 1c). From the fracture surface sample (not shown), it can be seen that the depth was about 300nm in average. As expected, a hierarchical hybrid micro/nano structure was observed on the surface of Micro-nano-Ti samples (Fig. 1d). There is no significant difference in the surface morphology under low magnifications between the Micro-Ti (Fig. 1b) and the Micro-nano-Ti samples (Fig. 1d). However, the well-developed nanotube array structure can be found in the higher magnification image (inset of Fig. 1d), which is similar to that observed on the surface of the Nano-Ti sample (Fig. 1c). This means that the combined uses of acid etching and anodic oxidation can integrate their individual topographic characteristics in one Ti sample. The SEM images proved that we successfully produced Ti samples with four different types of surface topographies: with neither nanoscale nor microscale topographic features (Fig. 1a), with only microscale topographic features (Fig. 1b), with only nanoscale topographic features (Fig. 1c), and with both micro- and nanoscale topographic features (Fig. 1d).

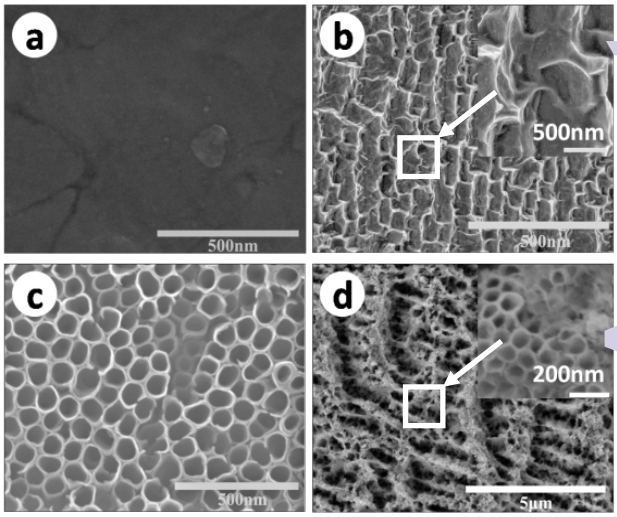

Figure 1. Surface morphologies of the polished Ti (a), Micro-Ti (b), Nano-Ti (c), and Micro-nano-Ti (d). Insets are the high magnification view of the selected area marked with white rectangles.

XPS was used to characterize the surface chemical composition of the Ti sample after treatment. The results are shown in Figure 2. From XPS survey spectrum (Fig. 2a), it can be seen that F, C and N elements also appear on the treated Ti surface. Among them, C and N are from organic contamination, while the F element is from the electrolyte used in the anodization process. The peaks in the Ti2p spectrum (Fig. 2c) can be assigned to Ti(IV)-O bonds and that in the O1s spectrum (Fig. 2b) is corresponding to the O-Ti(IV) bonds, indicating that the Ti sample was oxidized after the surface treatment.

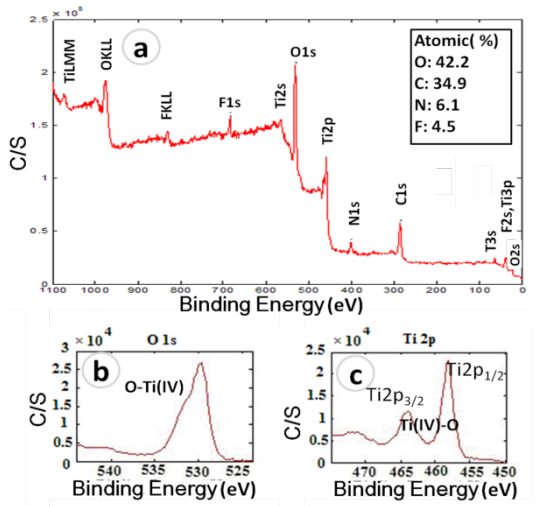

Figure 2. XPS spectra of the Ti surface after acidic treatment and anodization: (a), survey spectrum: (b), O1s spectrum and (c), T2p spectrum.

Besides surface topography, surface roughness and hydrophilicity are also of great importance in affecting osteoblast behaviors.[6] The surface roughness of the samples was measured using AFM (shown in Fig. 3), and the hydrophilicity was evaluated by contact angle measurements (shown in Fig. 4). The root-mean-square surface roughness of the polished Ti, Micro-Ti, Nano-Ti, and Micro-nano-Ti surfaces was 40±5nm, 180±10nm, 53±3nm and 100±4nm, respectively. As expected, the Micro-Ti and the Micro-nano-Ti showed higher surface roughness due to the formed micro-sized erosion pits whereas the polished and the Nano-Ti exhibited lower roughness. The water contact angle of these samples was 90°±1° for the polished Ti, 82°±4° for the Micro-Ti, 41°±5° for the Nano-Ti and 61°±5° for the Micro-nano-Ti. Compared to the polished Ti and the Micro-Ti, the Nano-Ti and the Micro-nano-Ti showed enhanced hydrophilicity, suggesting that the anodic oxidation had a more significant effect on the surface hydrophilicity, compared to the acid etching. These results also indicate the significant effects of the nanostructures on the hydrophilicity.

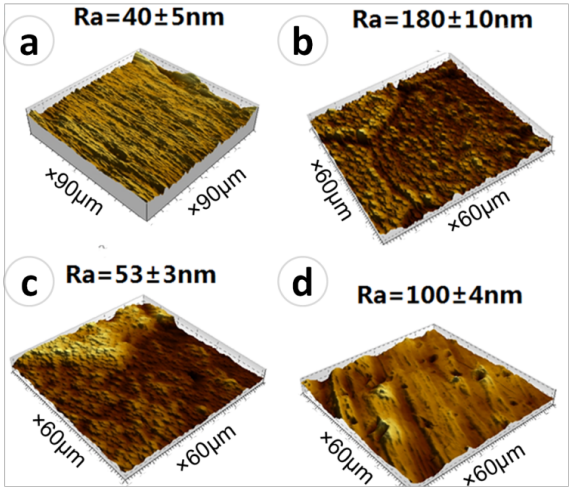

Figure 3. The surface roughness of the polished Ti (a), Micro-Ti (b), Nano-Ti (c), and Micro-nano-Ti (d).

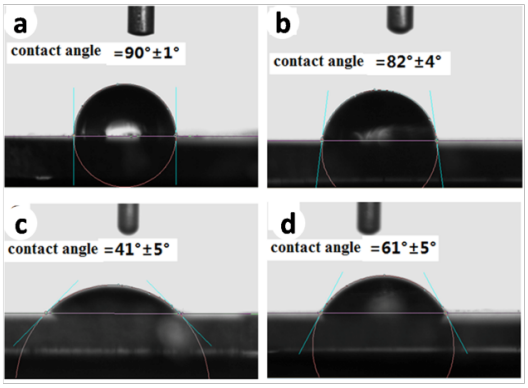

Figure 4. The surface hydrophilicity of the polished Ti (a), Micro-Ti (b), Nano-Ti (c), and Micro-nano-Ti (d).

Figure 5 represents the surface morphologies of the polished Ti, Micro-Ti, Nano-Ti, and Micro-nano-Ti after immersion in SBF for 2 weeks. It can be seen that there was no obvious difference in the surface morphologies of the polished Ti and the Micro-Ti before and after immersion (Fig. 5a, 5b), indicating that no Ca-P compounds was formed on their surface. By contrast, for the Nano-Ti and Micro-nano-Ti, a new layer of substance was uniformly formed on their surfaces, making the initial surface nanostructure (Fig. 5c) and microstructure invisible (Fig. 5d). The newly formed substance was proved to mainly consist of Ca and P by EDS (inset in Fig. 5d). Considering that the most prominent difference between the samples with Ca-P deposits and those without is the surface nanostructure, it is reasonable to conclude that the nanostructure plays an important role in the promotion of Ca-P mineralization in SBF. It is well-known that the Ti surface produced by anodic oxidation is rich of hydroxyl groups (Ti-OH), which can make the surface negatively charged [19]. The Ti–OH group has been well-documented to promote the Ca-P mineralization in SBF [20]. In SBF, the H from the hydroxyl group is released as a free proton, with the remaining O carrying a negative charge. This negative charged surface attracts positively charged calcium ions (Ca^{2+}) from the SBF, followed by the arrival of negative charged phosphate groups (HPO_4^{2-}). As a consequence, a layer of Ca-P compounds is formed on the surface, which then transforms into the bone-like apatite. Therefore, the more amount of –OH groups a surface has, the stronger ability to induce Ca-P mineralization the surface will have. In this study, the nanostructure formed by the anodic oxidation is actually acting as an "enhancer", to magnify the effects of –OH, as the nanostructure has a high surface specific area, causing a significant increase in the –OH group density. This higher density of the –OH group is a possible reason for the enhanced hydrophilicity of the Nano-Ti and the Micro-nano-Ti (Fig. 5c and 5d). The SBF immersion test has been widely used to predict the in-vivo bone formation ability, and it has been proved that in most of cases, it can successfully predict the relative performance of biomaterials in vivo [21]. Therefore, the immersion results indicate the better potential of the Nano-Ti, and Micro-nano-Ti for inducing bone formation in vivo. In this study, nanostructured Ti surface showed enhanced hydrophilicity and bioactivity, which confirmed the

beneficial effect of hydrophilicity on bioactivity, and is also consistent with the previously reported data by other researchers.[6]

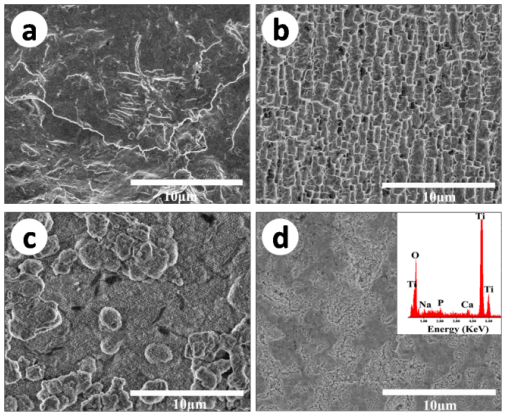

Figure 5. The surface morphology of the polished Ti (a), Micro-Ti (b), Nano-Ti (c), and Micro-nano-Ti (d) after immersion in SBF for 2 weeks. The Inset in (d) is the EDS spectrum of the deposits formed on the surface.

The cell proliferation on the polished Ti, Micro-Ti, Nano-Ti, and Micro-nano-Ti surfaces is shown in Fig. 6. It can be seen that, over 7 days of incubation, the cells showed a time-dependent growth pattern on all the samples. At day 1, the cell number on the polished Ti was the least, followed by that on the Micro-Ti. However, there was no statistically significant difference in the cell number between the Nano-Ti and the Micro-nano-Ti. By day 4, significant increase in cell numbers on all the samples was observed. The cells proliferated most quickly on the Micro-nano-Ti, followed by those on the Nano-Ti, and the cell number on the Micro-Ti was still more than that on the polished Ti. By day 7, the cell proliferation rate showed a similar trend to those observed at day 4. The cell number on the Micro-nano-Ti was slightly larger than that on the Nano-Ti, both were about 2-fold that on the polished Ti. The cell number on the Micro-Ti is about 0.5-fold higher than that on the polished Ti.

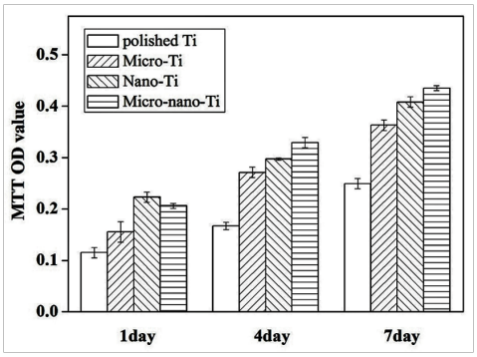

Figure 6. MTT assay results representing the MC3T3-E1 cell proliferation on the polished Ti, Micro-Ti, Nano-Ti, and Micro-nano-Ti.

The morphologies of MC3T3-E1 cells on the polished Ti, Micro-Ti, Nano-Ti, and Micro-nano-Ti surfaces after culturing for 1 day are displayed in Fig. 7. It shows that most of the cells cultured on the four types of sample surfaces become flattened after incubation of 1 day. However, difference in the cell morphology can be observed. Most of the cells on the polished Ti show a bi- or a tri-polar spindle-like morphology (Fig. 7a), while those on the Micro-Ti showed a polygonal-shaped morphology (Fig. 7b). In contrast, the cells on the Nano-Ti and the Micro-nano-Ti surfaces exhibited a polygonal shape with many filopodia extending from the cell body (Fig. 6c and d).

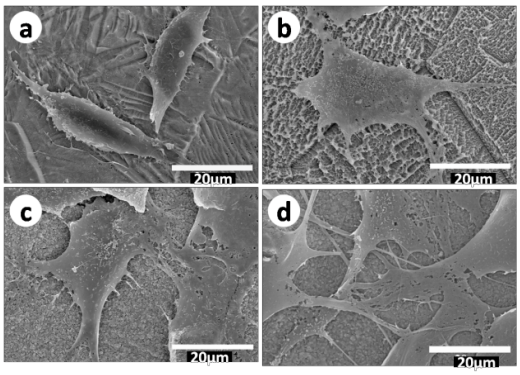

Figure 7. the morphologies of MC3T3-E1 cells cultured for 1 day on the polished Ti (a), Micro-Ti (b), Nano-Ti (c), and Micro-nano-Ti (d).

Among the osteogenic marker, bone sialoprotein (BSP) plays an important role in promoting osteoblast adhesion, and differentiation.[22] In vitro study showed that, in osteoblast cells, increase in BSP gene expression can stimulate the expression of other osteogenic genes including runt-related transcription factor 2 (Runx2), Osterix (Osx), alkaline phosphatase (ALP) and osteocalcin (OCN), and, in turn, increase matrix mineralization.[23] Figure 8a shows the gene expression level of BSP in cells after culturing for 7 days. It can be seen that, compared to cells on the polished Ti, higher mRNA levels of BSP were detected in the cells cultured on the Micro-Ti, Nano-Ti and Mirco-nano-Ti surfaces. In contrast, the mRNA level of GAPDH, the housekeeping gene, showed no changes among the four samples. To further quantify the BSP gene expression, quantitative real-time PCR was performed. As shown in Fig. 8b, the gene expression level of BSP mRNA in the MC3T3-E1 cultured on the Micro-Ti, Nano-Ti and Mirco-nano-Ti was significantly higher than that on the polished Ti (p<0.05). Compared to the polished Ti, the Micro-Ti and the Nano-Ti increased the BSP mRNA levels by 1.9-fold and 1.6-fold respectively, while the Micro-nano-Ti increased the BSP mRNA levels by 3.0-fold, suggesting the more significant influence of the Micro-nano-Ti on the gene expression of osteoblasts. The upregulated expression of this bone specific gene together with the better adhesion and the enhanced proliferation indicate the best biocompatibility of the Micro-nano-Ti, by contrast, the biological results in this study revealed that the polished Ti had the worst biocompatibility, which indicates the importance of both micro and nanostructure for the cytocompatibility. The microscale and nanoscale topographic features are both well-accepted to benefit the osseointegration of bone implants.[24] It has been reported that the microstructure is beneficial for the formation of the mechanical interlocking of the implant with the bone.[3] The

nanostructure has more prominent influence on the initial cell behaviors. Bone cells sense the underlying surface by their cytoskeletal projections (filopodia and lamellipodia). The focal adhesion formed between cells and the substrate surface can mediate the mechanotransductive signaling from the underlying surface. TiO_2 nanotubes are one of the most widely used nanotopographical features to manipulate the cell behaviors. Brammer et al. [25] revealed that TiO_2 tubes facilitated cell probing, sensing and migration of primary bovine aorta endothelial cells. However, the effects of nanotube on the cellular behavior is size-dependent.[26] Therefore, to maximize the enhancement on the osseointegration, a series of work should be done in future to figure out the optimized tube dimensions which best match with the microstructure produced by the acid etching.

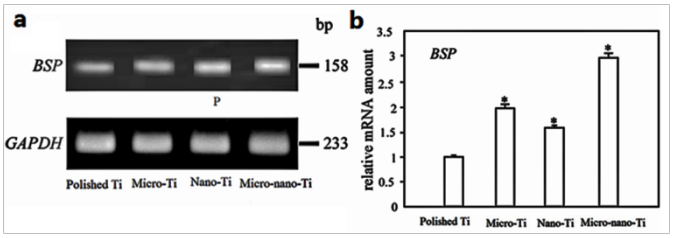

Figure 8.RT-PCR (a) and Real-time PCR (b) analysis of BSP mRNA levels in MC3T3-E1 cells cultured for 7 days on the polished Ti, Micro-Ti, Nano-Ti, and Micro-nano-Ti. * indicates a p value < 0.05.

Besides the surface topographic features, researchers also demonstrated the beneficial effects of surface roughness and hydrophilicity on cell behaviors, such as early stage differentiation and bone cell proliferation.[3,20] In this research, the acid etching produced the microstructure, increasing the surface roughness (Fig. 3), while the anodic oxidation generated the nanostructure, enhancing the surface hydrophilicity (Fig. 4). Both advantages of the increased surface roughness and enhanced surface hydrophilicity are combined together in the Micro-nano-Ti, which possibly accounts for its better biocompatibility, compared to the other samples. In summary, we, in this study, pointed out the importance of the synergistic effect of both micro and nanostructure on the in-vitro Ca-P mineralization and osteogenic functions of the osteoblasts. Besides, it should be highlighted the potential of the combination of two simple and cost-effective surface techniques to amplify their enhancement on the biological performance of bone implants.

Conclusion

The hierarchical hybrid micro/nanostructure was produced on the surface of Ti implants to improve their bioactivity. Acid etching produced a microstructure while anodic oxidation generated a well-aligned nanotubular structure. Both micro- and nanotopographic features were perfectly integrated on Ti surfaces through the combination of these two simple and cost-effective surface techniques. Results showed that the Ti surface with the hybrid micro/nanostructure had an enhanced hydrophilicity and promoted the Ca-P mineralization in SBF. Moreover, the hybrid micro/nanostructure was also revealed to be capable of promoting the osteoblast adhesion and proliferation, and upregulated the expression of the osteogenic marker (bone sialoprotein). This study points out the significant importance of synergistic effects of the micro- and nanotopographic features on the biological performance of the bone implants, providing insights into the surface engineering of bone-related biomaterials.

Acknowledgements

The authors gratefully acknowledge the support by the National Natural Science Foundation of China (Project No.51201056, No.51171058, No.51401146), Natural Science Foundation of Hebei Province of China (Project No.E2013202021, No.E2013202022), Science and Technology Plan Project of Hebei Province (No.13211027) and Science and Technology Correspondent Project of Tianjin (No. 14JCTPJC00496).

Notes and references

1 K. Mustafa, A. Wennerberg, J. Wroblewski, K. Hultenby, B. Silva Lopez and K. Arvidson, *Clin. Oral Impl. Res.*, 2001, 12, 515.
2 J. Tan, H. Shen and W.M. Saltzman, *Biophys J*, 2001, 81, 2569.
3 Y. Ito, *Biomaterials*, 1999, 20, 2333.
4 C.D.W. Wilkinson, *Mater. Sci. Eng. C*, 2002, 19, 263.
5 Y. Li, B. Li, X. Fu, J. Li, et al., *J. Hard Tissue Biol.*, 2013, 22, 351.
6 B. Li, Y. Li, J. Li, X. Fu, et al., *J. Mater. Sci.: Mater. Med.*, 2014, 25, 199.
7 L. Gao, B. Feng, J. Wang, X. Lu, D. Liu, S. Qu and J. Weng, *J. Biomed. Mater. Res. B*, 2009, 89B, 335.
8 L. Zhao, S. Mei, P.K. Chu, Y. Zhang and Z. Wu. *Biomaterials*, 2010, 31, 5072.
9 M. Monjo, S.F. Lamolle, S.P. Lyngstadaas, H.J. Ronold and J.E. Ellingsen. *Biomaterials*, 2008, 29, 3771.
10 X. Liu, P.K. Chu and C. Ding, *Mater. Sci. Eng. R*, 2010, 70, 275.
11 S. Minagar, J. Wang, C.C. Berndt, E.P. Ivanova and C. Wen, *J. Biomed. Mater. Res. Part A*, 2013, 101A, 2726.
12 J. Tan and W.M. Saltzman, *Biomaterials*, 2004, 25, 3593.
13 K. Kubo, N. Tsukimura, F. Iwasa, T. Ueno, L. Saruwatari, H. Aita, et al. *Biomaterials*, 2009, 30, 5319.
14 Y. Xie, H. Ao, S. Xin and X. Zheng, *Mater. Sci. Eng. C*, 2014, 38, 272.
15 G. Balasundaram, C. Yao and T.J. Webster, *J. Biomed. Mater. Res. A*, 2008, 84A, 447.
16 T. Hanawa, *Mater. Sci. Eng. C*, 2004, 24, 745.
17 T. Kokubo, H. Kushitani, S. Sakka, T. Kitsugi and T. Yamamuro, *J. Biomed. Mater. Res.*, 1990, 24, 721.
18 D. Gerlier and N. Thomasset, *J. Immunol. Methods*, 1986, 9, 457.
19 M.C. Advincula, F.G. Rahemtulla, R.C. Advincula, E.T. Ada, J.E. Lemons and S.L. Bellis, *Biomaterials*, 2006, 27, 2201.
20 B.Li, Y. Li, J. Li, et al., *Appl. Surf. Sci.*, 2014, 37, 202.
21 A. Zadpoor, *Mater. Sci. Eng. C Mater. Biol. Appl.*, 2014, 35, 134.
22 B. Ganss, R.H. Kim and J. Sodek, *Crit. Rev. Oral Biol. Med.*, 1999, 10, 79.
23 J.A. Gordon, G.K. Hunter and H.A. Goldberg, *Cells Tissues Organs*, 2009, 189, 138.
24 J. Tan and W.M. Saltzman. *Biomaterials*, 2004, 25, 3593.

25 K.S. Brammer, S. Oh, J.O. Gallagher and S. Jin, *Nano Lett.*, 2008, 8, 789.
26 N. Wang, H. Li, W. Lü, et al., Biomaterials, 2011, 32, 6900.

Table 1 Primers for RT-PCR and Real-time PCR

Gene	Gene bank ID	DNA primer	Sequence	Size (bp)
GAPDH	**NM_008084.3**	Forward	5’- GGTGAAGGTCGGTGTGAACG-3’	233
		Reverse	5’-CTCGCTCCTGGAAGATGGTG-3’	
BSP	**NM_008318.3**	Forward	5’-CAGGGAGGCAGTGACTCTTC-3’	158
		Reverse	5’-AGTGTGGAAAGTGTGGCGTT-3’	